Journal of Catalysis **189,** 184–194 (2000)
Article ID jcat.1999.2693, available online at http://www.idealibrary.com on IDEAL®

Hydrogenation of Aromatics on Sulfur-Resistant PtPd Bimetallic Catalysts

R. M. Navarro,* B. Pawelec,* J. M. Trejo,† R. Mariscal,* and J. L. G. Fierro*,[1]

*Instituto de Catálisis y Petroleoquímica, CSIC, Cantoblanco, 28049 Madrid, Spain; and †Repsol, S.A., Embajadores 183, 28045 Madrid, Spain
E-mail: jlgfierro@icp.csic.es

Received July 2, 1999; revised September 2, 1999; accepted September 2, 1999

Silica–alumina (SA)-supported Pt, Pd, and PtPd catalysts were compared for the hydrogenation of toluene and naphthalene in the presence of dibenzothiophene (DBT). The relative intrinsic hydrogenation activity suggested that PtPd catalysts are very active with respect to their monometallic (Pt and Pd) counterparts. The greater resistance of PtPd samples to poisoning by sulfur compounds was confirmed by dosing variable amounts (113–1200 ppm) of DBT into the feed. The structure of the catalysts was revealed by Fourier transform infrared spectroscopy (FTIR) of chemisorbed CO, temperature-programmed reduction (TPR), and X-ray photoelectron spectroscopy (XPS) techniques. TPR, FTIR, and XPS analyses of bimetallic catalysts revealed the strong Pt–Pd interaction in the bimetallic particles formed. Structural analysis of the used bimetallic sample indicated that the electro-deficient character of platinum (isolated Pt clusters on the Pd surface) is responsible for the strong sulfur resistance of the PtPd samples.

Key Words: **aromatics hydrogenation; thioresistance; Pt and Pd catalysts.**

INTRODUCTION

Deep hydrogenation (HYD) of aromatics and deep hydrodesulfurization (HDS) in diesel fuel are the focus of many recent studies owing to environmental and clean-fuel legislation (1–4). These studies indicate that the extent of particulate emissions in diesel exhaust gases can be reduced by: (i) decreasing the sulfur content of the fuel, (ii) increasing the number of cetane, and (iii) decreasing the aromatic content (2). The latter two strategies are, to a certain extent, interrelated: for example, reducing the content of aromatics has a positive effect on the cetane number (5). Beginning in the year 2000, methods for meeting specifications for diesel fuels will include reducing sulfur to 50 ppm and setting the number of cetane from 51 to 58 (this means an aromatics content of 10 to 20 vol%) (4). To meet these strict standards for diesel fuels, oil refineries must make use of new catalytic systems and hydrotreating processes.

Two approaches—a single-stage process and a two-stage process—have been proposed for meeting the above-mentioned requirements. The single-stage process, which combines severe HDS with HYD using a single conventional CoMo, NiMo, or NiW catalyst, reaches the necessary aromatic saturation only at H_2 pressures substantially higher than the H_2 pressure at which current HDS units operate (6). The two-stage system, which uses a hydrotreating catalyst in the first reactor and a platinum-supported catalyst in the second, yields a low aromatic diesel stream at moderate hydrogen pressure (7, 8). This system is highly active for the reduction of aromatics but is very susceptible to sulfur poisoning (9). Accordingly, the sulfur concentration at the inlet of the second reactor must be decreased to a few parts per million (3). Thus, the use of these catalysts is limited by the severe pretreatment conditions, unless sulfur tolerance can be greatly improved.

Considerable attention has, therefore, been paid recently to developing catalysts with a high hydrogenation activity while at the same time maintaining strong resistance to poisoning through the small amounts of sulfur present in the feed stream. Since the mechanism of metal poisoning by sulfur compounds involves strong chemisorption of the S-containing molecule on the metal sites followed by its hydrogenolysis (as represented by the equilibrium: $Me^o + H_2S \Leftrightarrow Me\text{-}S + H_2$), the H_2S produced would probably lead to the formation of a stable and inactive Me–S species on the catalyst surface. However, this equilibrium may shift to the left-hand side when the hydrogen pressure is high, and/or when the physicochemical characteristics of the metal atoms are modified by: (i), alloying, (ii), changing the metal particle size, or (iii), changing the acid–base properties of the carrier (10). With respect to the latter, it was reported that the sulfur tolerance of Pt or Pd catalysts can be greatly enhanced by using acidic supports such as zeolites (2, 3, 6, 10–13), whereas less acidic supports, such as SiO_2–Al_2O_3, can generate moderate sulfur resistance (3, 14–16). It is believed that the high S-tolerance of zeolite-based Pt or Pd catalysts arises from the formation of electron-deficient metal particles, $Pt^{\delta+}$ or $Pt^{\delta+}$, upon interaction of the reduced metal with the Brønsted acid sites

[1] To whom correspondence should be addressed.

0021-9517/00 $35.00

of the zeolite, which in turn lowers the strength of the S–Me bond (13). The electron-deficiency of metal particles, which alters the metal–adsorbate bond strength, has been used to explain the significant changes in turnover frequencies of aromatic hydrocarbon hydrogenation on small Pt and Pd metal clusters in a zeolite framework (10, 12, 17–19). Since this explanation is difficult to apply to large metal crystallites, the electronic properties of which are probably similar to those of bulk metal (20), an alternative explanation for the enhanced activities of Pd and Pt, supported on acidic carriers, involves a Langmuir–Hinshelwood model, which invokes dual-site adsorption, both on the metal and on the support (15, 16, 21). However, Poondi and Vannice (20) noted a certain degree of internal inconsistency in this model and proposed an alternative that assumes the formation of hydrogen-deficient surface species.

Other studies have focused on the high sulfur tolerance of Pt, Pd, or PtPd catalysts supported on Al_2O_3, TiO_2, and SiO_2 (22–25). Current interest in bimetallic catalysts is increasing, in particular because they show superior selectivity and resistance to poisoning as well as improved activity and stability as confirmed by certain industrial processes. The patent literature shows that the combination of Pt and Pd, supported on alumina and zeolites, is effective for the hydrogenation of aromatics in petroleum feedstocks containing sulfur compounds (26–29). Yasuda and Yoshimura (6) confirmed that the coexistence of Pt and Pd in USY zeolite strongly enhances tetralin hydrogenation and improves sulfur tolerance, which depends on the Pd/Pt ratio and reaches a maximum value at a Pd : Pt molar ratio of 4 : 1. The high sulfur tolerance of the PdPt system was attributed to structural and electronic effects rather than to the degree of metal dispersion. A similar conclusion was reached by Koussathana *et al.* (22). However, the authors of both papers failed to present direct experimental evidence of the geometric or electronic modifications. Studies by Cooper and Donnis (3) revealed that the preparation of a PtPd bimetallic catalyst, and hence the degree to which Pt and Pd form alloyed clusters, as well as the particle size of these clusters strongly affect the activity as well as the sulfur tolerance of these catalysts. In contrast, Sinfelt (30) demonstrated that the ability of metals to form bulk alloys is not a necessary condition for their use as catalysts.

Accordingly, the main objective of the present work was to determine whether the sulfur tolerance of Pt improves when a second noble metal (Pd) is added to a silica–alumina (SA) substrate. This carrier was selected instead of zeolites in order to minimize the effect of coking on catalyst deactivation. The hydrogenation of toluene and naphthalene mixtures was chosen as a model reaction because: (i) on a given catalyst it is possible to compare the relative reactivity of the hydrocarbons, which depends on their molecular structure (31), (ii) both model compounds resemble the structure of aromatic compounds found in the diesel fraction (typical light gas oil (LGO)), and (iii) additional information can be obtained about the surface structure of the catalyst itself (12, 32). Dibenzothiophene (DBT) was selected as the model compound for sulfur poisoning because not only is its desulfurization chemistry known (33), but DBT is also one of the main S-containing compounds in diesel. Careful investigation of the catalyst structure was afforded by IR spectroscopy of chemisorbed CO, temperature-programmed reduction (TPR), CO chemisorption, and X-ray photoelectron spectroscopy (XPS) measurements in an attempt to establish a relationship between activity and the catalyst structure.

EXPERIMENTAL

Catalyst Preparation

A commercially available support, SiO_2–Al_2O_3 (hereafter abbreviated to SA), containing 28 wt% alumina (SMR 5-473, Grace Davison Chemical) was calcined in air at 773 K for 3 h prior to catalyst preparation. Pt/SA and Pd/SA catalysts were prepared by wet impregnation of the support with aqueous solutions of H_2PtCl_6 (Sigma) and $Pd(NO_3)_2 \cdot H_2O$ (Fluka, purity >98%), respectively. For this purpose, a known weight of the carrier was placed in a solution of the required amount of noble metal added to 100 ml of water, and the pH was fixed at a value close to 7. After adsorption equilibrium had been reached (after contact for 12 h at room temperature), excess water was removed in a rotary evaporator. Subsequently, the impregnate was dried at 383 K in air for 4 h and finally calcined in air at 573 K for 4 h. The Pt and Pd contents in monometallic catalysts were 0.51 and 1.04 wt%, respectively. The bimetallic PtPd/SA catalyst was prepared by simultaneous impregnation of the SA carrier using the adsorption–impregnation method and the same metal precursors as above. Chemical analysis revealed metal contents of 0.94 and 0.27% for Pd and Pt, respectively, and chlorine amounts of 0.01 to 0.02%, respectively.

Catalyst Characterization

The textural properties of the catalysts were evaluated from the nitrogen adsorption–desorption isotherms obtained at 77 K over the whole range of relative pressures, using a Micromeritics ASAP-2000 apparatus, for samples previously outgassed at 413 K for 18 h. BET surface areas were calculated from these isotherms using the BET method in the 0.005–0.25 P/P_o range. In all cases, correlation coefficients above 0.999 were obtained. Pd and Pt contents were determined using a Perkin-Elmer 3030 atomic absorption spectrophotometer.

Temperature-programmed reduction (TPR) experiments were carried out in a semiautomatic Micromeritics TPD/TPR 2900 apparatus interfaced to a microcomputer.

Prior to reduction, the catalysts (about 50 mg) were heated at a rate of 15 K/min up to a final temperature of 573 K and kept at that temperature for 1 h in a stream of air to remove water and other contaminants. Then, the catalysts were cooled to room temperature in the same flow of air. TPR profiles were obtained by passing a 10% H_2/Ar flow (50 mL/min) through the sample. Since PdO is an easily reducible oxide, even at room temperature, all TPR experiments were carried out after sample conditioning and further exposure to the H_2/Ar mixture at temperatures of 263 to 1273 K. The temperature was increased at a rate of 15 K/min, and the amount of H_2 consumed was determined with a thermoconductivity detector (TCD). The effluent gas was passed through a cold trap before the TCD in order to remove water from the exit stream.

Volumetric CO chemisorption isotherms at 298 K were obtained in order to estimate metal dispersion. Before the measurements, the sample was reduced under H_2 at 573 K for 1 h and then outgassed at 10^{-5} Torr (1 Torr = 133.33 Pa). After cooling the sample to 293 K, CO was admitted and the first adsorption isotherm was measured. After evacuation for 15 min at room temperature, a second isotherm was measured. The difference between the first and the second isotherm, extrapolated to zero pressure, gives the amount of strongly chemisorbed CO. The dispersion was calculated assuming a stoichiometry of adsorption of $CO/M_S = 1$ (M = Pt), 0.68 (M = Pd), and 0.82 (M = PtPd).

Photoelectron spectra were recorded on a VG Escalab 200R electron spectrometer equipped with a hemispherical electron analyzer, using a Mg$K\alpha$ ($h\nu = 1253.6$ eV, 1 eV = 1.603×10^{-19}) 120-W X-ray source. A PDP 11/04 computer (Digital Equipment) was used to record and analyze the spectra. The samples used in the HYD reaction were kept in isooctane to avoid contact with air. All samples were mounted onto a manipulator, which allowed transfer from the preparation chamber to the analysis chamber. The reduction treatment was carried out *in situ* at 573 K for 1 h. After outgassing at 10^{-5} Torr, the prereduced or used samples were transferred to the ion-pumped analysis chamber, the residual pressure of which was kept below 7×10^{-9} Torr during data acquisition. The binding energy (BE) of the Si 2p peak of the support at 103.4 eV was taken as an internal standard. The accuracy of the BE values was ±0.1 eV. Each spectral region of the photoelectrons of interest was scanned a number of times to obtain a good signal-to-noise ratio. The intensities of the peaks were estimated by calculating the integral of each peak after subtracting an S-shaped background and fitting the experimental peak to a combination of Lorentzian/Gaussian lines of variable proportions.

The IR spectra of adsorbed CO were recorded with a Nicolet 5ZDX Fourier transform spectrophotometer working with a resolution of 4 cm^{-1} over the entire spectral range and averaged over 100 scans. The samples in the form of self-supporting wafers of 10 mg cm^{-2} were pretreated in an infrared cell designed to work under vacuum (a residual pressure of 10^{-5} Torr) or under dynamic conditions and fitted with greaseless stopcocks and KBr windows. The catalysts were reduced in flowing hydrogen at 573 K for 1 h and then outgassed at the same temperature for 1 h. All spectra were obtained upon adsorption of 30 Torr CO at room temperature, followed by evacuation for 10 min. The net infrared spectra were obtained by subtracting the sample background spectrum corresponding to CO gas and the cell windows from the whole spectrum.

Activity Measurements

Hydrogenation of aromatic compounds was performed in a continuous-downflow catalytic reactor (9.5 mm i.d. and 130 mm length). The model feed was prepared with a view to approaching the composition of conventional hydrotreated light atmospheric gas oil. Thus, it consisted of DBT, naphthalene, and toluene dissolved in hexadecane. In order to evaluate the sulfur tolerance of the PtPd sample, varying amounts of DBT were dosed into the feed. Hereafter, the samples will be abbreviated to PtPdx, where x denotes the amount of S (ppm) in the feed. Table 1 shows the composition of the feed used.

In order to avoid deviations from plug flow (34), activity tests were performed using 1 g of catalyst diluted with SiC (both in the 0.25- to 0.30-mm particle size range) at a volume ratio of 1 : 1. In addition, the top of the reactor was filled with SiC to aid liquid dispersion over the cross section of the catalyst bed. For activity tests, the catalysts were reduced *in situ* at atmospheric pressure in an H_2/N_2 mixture (ratio 1 : 10 vol). The reduction procedure consisted of heating to the reduction temperature of 573 K (heating rate 3 K/min) in an H_2/N_2 mixture (ratio 1 : 10 vol, a flow rate 55 ml/min) at atmospheric pressure and then isothermal reduction at this temperature for 2 h. Catalytic activities were measured at 468, 503, and 523 K, 5 MPa of total pressure, and weight hourly space velocity (WHSV) of 4.5 h^{-1}. The hydrogen-to-liquid feed ratio was set at 558 L(N)/L. The reaction was kept at steady state for 3.5 h. Liquid samples were collected for 15 min after stabilization. Subsequently, the reaction temperature was changed and

TABLE 1

Model Feed Composition Used in the Hydrogenation of Aromatics[a]

S (ppm)	113	299	626	1217
Total aromatics (%)	22.12	22.26	22.99	22.99
Mono (%)	20.04	20.10	20.62	20.33
Di (%)	2.01	1.99	2.00	1.96
S aromat (%)[b]	0.065	0.17	0.36	0.70

[a] Weight percentage.
[b] As DBT.

sampling was carried out in a similar manner after 3.5 h. A precise deactivation test was carried out on the PtPd catalysts using this feed with 1200 ppm of S for 1 week. The reaction conditions were the same as above. The operation method consisted of consecutive discontinuous cycles (each cycle lasted 10 to 20 h). The reaction was stopped after each cycle, leaving the catalyst in a flow of N_2 overnight.

Liquid samples were analyzed by GC with FID (Varian chromatograph Model Star 3400 CX) equipped with a 30 m × 0.53-mm DB-1 column (J&W Scientific). Besides unreacted model feed compounds (DBT, naphthalene, and toluene), biphenyl (BP), cyclohexylbenzene (CHB), tetralin, decalin, and methylcyclohexane were the only products detected. In order to compare the reactivity of naphthalene and toluene, the hydrogenation of these compounds was analyzed according to the pseudo-first-order kinetic equation (35, 36). Taking into account that there was an excess of hydrogen in the reactor, the reversible reaction of hydrogenation can be neglected and the integral rate equation used has the form

$$k_{\text{tol,naph}} = -\left(\frac{F_{\text{tol,naph}}}{m}\right)\text{Ln}(1-X),$$

where, $k_{\text{tol,napth}}$ is the pseudo-first-order reaction constant for toluene or naphthalene hydrogenation (h^{-1} g_{cat}), X is the toluene or naphthalene conversion, F is the molar flow of reactant (mol h^{-1}), and m refers to the metal atoms exposed per gram of catalyst (mol g_{cat}^{-1} determined by CO chemisorption).

For naphthalene, a sequential path (naphthalene–tetralin–decalins (*cis* + *trans*) was assumed and the consecutive kinetic constant for tetralin hydrogenation was calculated using

$$k_{\text{tetral}} = k_{\text{naph}}\left[1 + \frac{k_{\text{naph}}C_{\text{naph o}}}{C_{\text{tetral}}}\left(e^{-\frac{k_{\text{napth}}m}{F_{\text{naph}}}} - e^{-\frac{k_{\text{tetral}}m}{F_{\text{naph}}}}\right)\right],$$

where, k_{naph} is the pseudo-first-order rate constant for naphthalene hydrogenation (h^{-1} g_{cat}), C_{naph} is the initial naphthalene concentration (mol L^{-1}), C_{tetral} is the tetralin concentration (mol L^{-1}), F_{naph} is the molar flow of naphthalene (mol h^{-1}), and m refers to the metal atoms exposed per gram of catalyst (mol g_{cat}^{-1} determined by CO chemisorption).

RESULTS AND DISCUSSION

Chemical and Textural Properties of Catalysts

The metal content and physical properties of Pt, Pd, and PtPd catalysts are given in Table 2. The textural properties, evaluated from the nitrogen adsorption–desorption isotherms, clearly indicate a decrease in the sorption capacity of the SA carrier after Pt and/or Pd incorporation. As expected, the BET surface areas of the calcined catalysts were lower than that of the SA carrier and decreased dramatically for binary samples. The drop in the adsorbed volumes of N_2 at a relative pressure of $P/P_o = 0.2$, and consequently in the BET area and porosity, indicates that some of the micropores and/or the smaller mesopores become occupied or blocked by platinum and/or palladium. Apart from this general trend, no changes in the shape of the isotherms or in the hysteresis loops of the nitrogen adsorption–desorption isotherms were observed in any of the catalysts.

TABLE 2

Chemical Composition[a] and Textural Properties[b] for Oxidic Pt, Pd, and Pt–Pd/SA Catalysts

Catalyst/ support	Pt (Pd) (wt%)	BET ($m^2 g^{-1}$)	Total pore volume ($cm^3 g^{-1}$)	Pore diameter (nm)	V_{N2}[c] ($cm^3 g_{cat}^{-1}$)
SA oxi	—	394	0.74	7.5	118.4
Pt oxi	0.51	335	0.64	7.7	100.9
Pd oxi	1.04	330	0.65	7.8	99.5
PtPd oxi	0.27 (0.94)	293	0.52	7.2	88.5

[a] As measured from AAS; data of Pd given in parentheses.
[b] BET specific area, pore volume, and average pore diameter.
[c] Volume of nitrogen adsorbed at 77 K and $P/P_o = 0.2$.

Temperature-Programmed Reduction (TPR)

The TPR profiles of the monometallic (Pd and Pt) and the bimetallic (PtPd) samples are shown in Fig. 1. For comparison, the TPR pattern of the SA carrier is included in the same figure. The TPR profile, resulting from SA, shows two overlapping peaks of about 640, 960, and 1090 K, associated with a reduction in oxidic impurities in the carrier; it is irrelevant from a catalytic point of view. These peaks are found in the profiles of all the catalysts, although they are more prominent at lower temperatures, especially in the case of Pd/SA, as a consequence of a stronger reduction due to hydrogen activation produced on the metallic species of the previously reduced noble metal.

The TPR profile of the Pd sample shows a positive peak at 295 K and a negative one at 356 K. The former can reasonably be assigned to the Pd oxide species, while the latter is attributed to desorption of hydrogen from the decomposition of a bulk palladium hydride formed through H-diffusion into the Pd crystallites (37). In contrast, the TPR profile of the Pt sample shows a broad reduction band extending from 300 to 700 K. The broadening suggests the presence of several Pt species. Since a small amount of chlorine (0.01%) was still present in the calcined Pt/SA catalyst (impregnated with a solution of H_2PtCl_6), the TPR profile may include surface oxychloride species of the form $Pt(OH)_xCl_y$ and PtO_xCl_y, in addition to PtO_2 (34). The TPR profile of the bimetallic PtPd catalyst is not simply the sum of the monometallic Pt and Pd samples. The bimetallic reduction profile exhibits peaks typical of PdO reduction (295 K) and

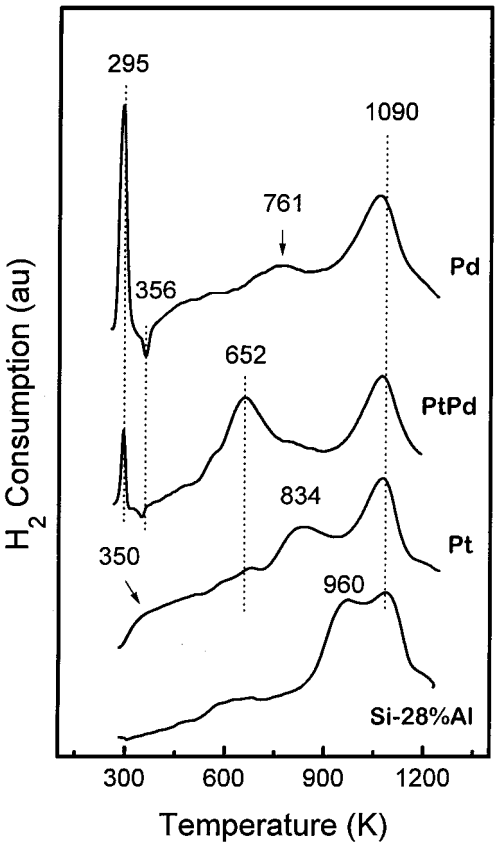

FIG. 1. Reduction profiles of oxidic Pt, Pd, and PtPd/SA catalysts as obtained from TPR with a 10% v H_2/Ar flow (50 ml min^{-1}) and a temperature gradient of 900 K h^{-1}.

subsequent Pd hydride decomposition (negative peak at 356 K), although both are much less intense than in the Pd sample. Since the amount of Pd content is about the same in both catalysts (Table 2), the decrease in H_2 consumption associated with the PdO species seems to depend on the presence of Pt. In addition, the second TPR peak around 652 K, detected in the PtPd sample indicates the reduction of Pd species together with the coimpregnated Pt, due to some kind of interaction with the latter. Similar interactions in PtPd systems were reported in TPR studies performed by Noronha *et al.* (38).

CO Chemisorption by FTIR

Chemisorption of CO was used to reveal the nature of the metal surface sites in reduced catalysts. The IR spectra of CO chemisorbed on the Pd, Pt, and PtPd catalysts are shown in Fig. 2. The infrared spectrum of CO adsorbed on the Pd catalyst displays two intense absorption bands at 1962 and 2108 cm^{-1}, corresponding to carbon monoxide bonded to surface palladium atoms in bridged and linear forms, respectively (39). As shown in Fig. 2, the IR spectrum of CO chemisorbed on the Pt catalyst is quite complex. In contrast to the Pd sample, the Pt catalyst shows a multiple linear CO absorption band between 1990 and 2080 cm^{-1}. The multiple absorption observed suggests that the reduced Pt/SA sample contains Pt^o species (CO linear band at 2050 cm^{-1} (40)) and platinum species in an electron-deficient state (CO linear band at 2080 cm^{-1} (41)). As the reduced Pt/SA catalyst still contains a small amount of chlorine species on the surface, this could be responsible for the multiple absorption band of CO chemisorbed on the Pt/SA sample (35).

The bimetallic catalyst exhibits two clear bands corresponding to linear adsorbed CO (at 2100 cm^{-1}) and bridging adsorbed CO (at 1950 cm^{-1}). The band corresponding to linear chemisorbed CO includes the contributions of CO bonded to surface Pd (2055 cm^{-1}) and Pt (2103 cm^{-1}) atoms. The intensity of the band of the Pt contribution is higher than the total band intensity in the Pt/SA spectra, despite the lower Pt content of the bimetallic sample. Compared to the Pt and Pd/SA catalysts, the bands at high wavenumber increased in intensity and the bridging CO bands decreased. Taking into account that carbon monoxide adsorbs onto the Pd surface in the bridging structure, some linear species appear if the pressure of the CO is increased (42), and, as stated above, the Pt metal absorbs CO mainly in a linear configuration. The integrated intensity band of CO bonded in bridging form on palladium in PtPd/SA (1.39 au) decreased with respect the monometallic Pd/SA (1.57 au),

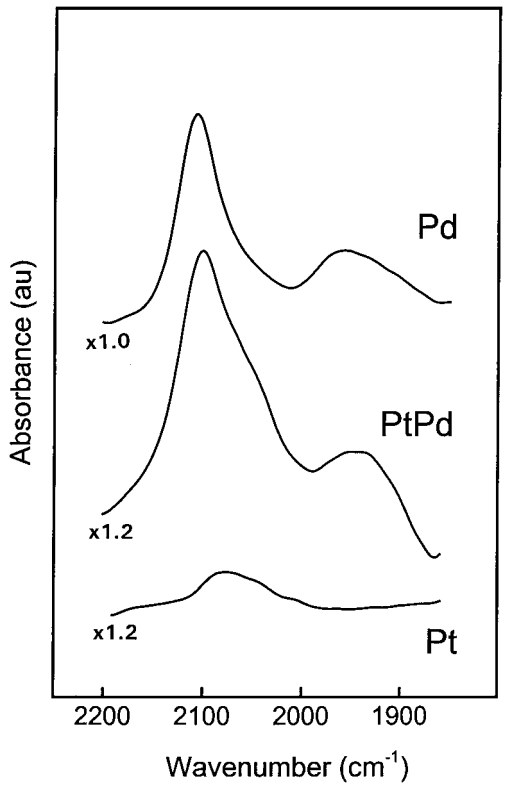

FIG. 2. Infrared spectra of CO chemisorbed on reduced Pt, Pd, and PtPd/SA catalysts. The CO gas phase was removed at 298 K. Gain is given in the spectra.

indicating that the Pd–Pd bond decreased in number by the formation of mixed Pt–Pd metal surface sites in the bimetallic PtPd/SA catalyst. The downward shift of the CO bands adsorbed on Pd (2055 and 1955 cm^{-1}) is also evidence of this decreasing coverage by CO (43).

X-ray Photoelectron Spectroscopy (XPS)

The energy regions of Si 2*p*, Al 2*p*, Pd 3$d_{5/2}$, Pt 4$d_{5/2}$, and S 2*p* core levels (in used samples) were scanned. Although the most intense photoemission lines of platinum are those arising from Pt 4*f* core levels, this energy region became overshadowed by the presence of a very strong Al 2*p* peak. Consequently, the energy region of the less intense Pt 4*d* peak was scanned for all the Pt-containing samples.

The binding energies of core electrons and the surface atomic ratios of freshly reduced and used Pd(Pt)/SA catalysts are summarized in Table 3 (see also Fig. 3). For the reduced Pd catalyst, the binding energy of the Pd 3$d_{5/2}$ level appeared at 335.4 eV and was assigned to Pd^o, in agreement with that obtained for a sputter-cleaned palladium foil (44). For the freshly reduced PtPd catalyst, a decrease in the Pd 3$d_{5/2}$ signal together with a positive binding energy shift to 336.0 eV was found. Neither structural changes associated with different metal loadings (44) nor support interaction effects were observed in the monometallic Pd sample. Thus, the observed positive shift may arise from changes in the electronic relaxation energy of Pd levels (45) in the presence of platinum, since an electron transfer from the Pd to the Pt *d*-electron population appears to be a crude approximation. This intimate Pt–Pd contact also accounts for the observed decrease in the surface exposure of Pd due to the dilution effect of Pt on the bimetallic particles formed. However, the decrease in the surface exposure of Pd is larger than the value expected for the Pt/Pd atomic ratio introduced, indicating some Pt surface segregation in the bimetallic particles. With respect to the freshly reduced bimetallic sample, the severely sulfur-poisoned sample (PtPd 1200 ppm S) shows a smaller shift in binding energy at the Pd 3$d_{5/2}$ level: 335.8 eV compared with 336.0 eV for the freshly reduced sample. This observation suggests a modification of the original electronic properties of bimetallic particles when the catalyst comes into contact with sulfur. It is surprising that no S 2*p* peak was detected for any of the spent monometallic (Pt and Pd) and bimetallic (PtPd) catalysts. With the sulfur level used in the feed, it is unlikely that the catalyst would have remained strictly metallic; thus, the absence of sulfur in the used samples suggests the decomposition of weakly bonded S on the catalyst surface during the vacuum pretreatment in the analysis chamber of the spectrometer.

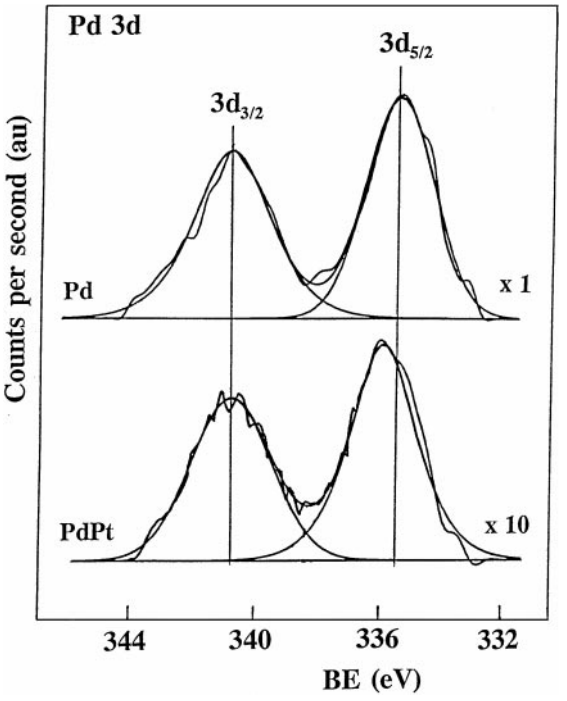

FIG. 3. Pd 3$d_{5/2}$ core level spectra of reduced Pd and PtPd samples.

TABLE 3

Binding Energies (eV) of Core Electrons and Surface Atomic Ratios of Reduced and Used Pd and PtPd Catalysts[a]

Catalyst	Pd 3*d* (eV)	(Si/Al) at	(Pd/Si) at
Pd red.	335.4[b]	2.43	0.046
Pd used[c] (100 ppm S)	335.3	2.21	0.049
PdPt red.	336.0	2.52	0.003
PtPd[c] (100 ppm S)	336.0	2.34	0.004
PtPd[c] (1200 ppm S)	335.8	2.59	0.004

[a] Neither Pt 3$d_{5/2}$ nor Pt 4*f* peaks were detected in Pt and PtPd/SA samples.

[b] A value of 335.4 eV was found for sputter-cleaned Pd foil (44).

[c] No S 2*p* was observed in used samples.

Toluene and Naphthalene Hydrogenation

Table 4 presents the activities of the Pt, Pd, and PtPd/SA catalysts in the hydrogenation of toluene and naphthalene performed under moderate operating conditions ($T = 468$ K, $P = 5.0$ MPa, WHSV $= 4.5$ h^{-1}, $S = 113$ ppm as DBT). For the three catalytic systems, the order of aromatic reactivity follows the sequence: naphthalene $\gg$ toluene > tetralin. This progression of rates corresponds to previous findings (46) and is clearly related to a decrease in the resonance energy per aromatic ring as well as to differences in the π-electron cloud density in the aromatic ring as result of the inductive effect of the methyl group (47). Of the catalysts tested, the bimetallic PtPd catalyst shows the highest intrinsic hydrogenation activity for the hydrogenation of naphthalene, tetralin, and toluene in the presence of 113 ppm of S, while Pt/SA clearly has the lowest intrinsic activity. Compared to Pd/SA, tetralin hydrogenation over PtPd/SA was enhanced by a factor of 6, whereas toluene

TABLE 4

Pseudo-First Rate Constants[a] for Naphthalene and Toluene Hydrogenation on Pt, Pd, and PtPd/SA Catalysts

	Catalyst: Pt/SA Dispersion[b]: 0.32			Pd/SA 0.15			PtPd/SA 0.15		
	Conv. (%)	K (h^{-1} g_{cat}^{-1})	Relative rate constant[c]	Conv. (%)	K (h^{-1} g_{cat}^{-1})	Relative rate constant[c]	Conv. (%)	K (h^{-1} g_{cat}^{-1})	Relative rate constant[c]
Naphthalene	76.4	121.6[d]	1	99.3	235.6[d]	1.93	99.7	266.1	2.19
Tetralin	(99.9[d,e])	0.06[d]	4.93×10^{-4}	(83.5[d,e])	8.6[d]	7.07×10^{-2}	(30.5[d,e])	54.6[d]	0.45
Toluene	0.14	1.62	1.33×10^{-2}	7.1	47.3	0.39	20.7	154.6	1.27
HDS (conv. %)		30.4			83.2			100	

[a] Measured at 468 K, total pressure 5 MPa, WHSV = 4.5 h^{-1}, $S = 113$ ppm as DBT.
[b] Measured from CO chemisorption.
[c] Relative to naphthalene hydrogenation on Pt/SA.
[d] A sequential path is assumed: naphthalene → Tetralin → Decalins (*cis* + *trans*).
[e] Selectivity to tetralin.

hydrogenation was increased by a factor of 3. Therefore, a synergetic effect between Pt and Pd in the PtPd/SA catalyst occurred during the aromatic hydrogenation reaction in presence of sulfur. This enhancement in the hydrogenation capacity aids in DBT dearomatization into a dihydro compound and its additional hydrogenation steps (48) and thus, the same activity trends appears for HDS and hydrogenation reactions.

Thioresistance of the PtPd/SA Catalyst

To elucidate the origin of the thioresistance of the bimetallic PtPd catalyst, the activity response of this system was studied for increasing concentrations of S in the feed (113–1200 ppm). The evolution of pseudo-first-order reaction constants in the hydrogenation of naphthalene, tetralin, and toluene at 468 K for varying sulfur contents in the feed is shown in Fig. 4. As expected, an increase in the sulfur concentration led to a decrease in the intrinsic activity of naphthalene, tetralin, and toluene hydrogenation. This inhibitory effect was more pronounced in the hydrogenation of toluene and tetralin. The increase in the sulfur content, from 113 to 1200 ppm, led to a decrease of 94 to 96% in the intrinsic activity; in the case of toluene and tetralin, there was a decrease of only 20% in naphthalene hydrogenation.

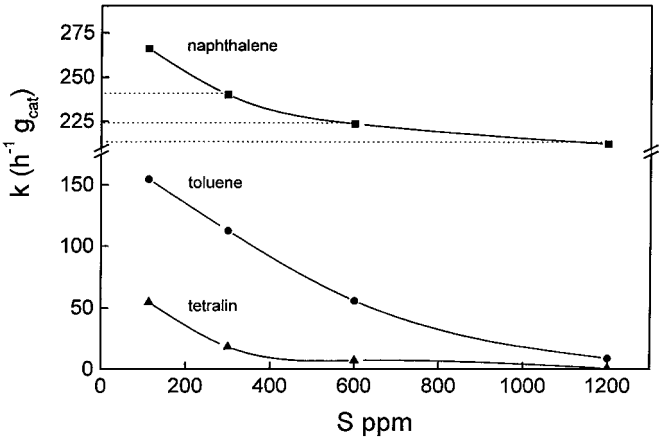

FIG. 4. Evolution of the pseudo-first-order rate constants for naphthalene (square), tetralin (top triangle), and toluene (circle) hydrogenation on the PtPd/SA catalyst with sulfur in the feed (113–1200 ppm). Reaction conditions were: $T = 468$ K, $P = 5$ Mpa, and WHSV = 4.5 h^{-1}.

The effect of temperature was investigated to obtain more information about this inhibitory effect on the saturation of monoaromatics. Figures 5 and 6 show the Arrhenius plots of toluene and tetralin hydrogenation, respectively, for increasing concentrations of sulfur in the feed (300–1200 S ppm). The Arrhenius parameters are shown in Table 5. Whereas tetralin hydrogenation, and toluene hydrogenation for a sulfur content of 1200 ppm, shows a temperature-independent activation energy, toluene hydrogenation behaves differently (Fig. 5). During the 300 to 600 S ppm interval, the apparent activation energy of toluene hydrogenation decreases at high temperature. This suggests the occurrence of pore diffusion limitation at high temperature. However, experiments with different particle sizes (from 0.12 to 0.68 mm) of catalysts revealed that, at these high temperatures, no limitation occurred. Therefore, since the overall apparent activation energy is a composite parameter including adsorption terms, the decrease in the apparent activation energy with increasing temperature can be associated with a decrease in surface coverage by toluene (49). On the other hand, toluene is a better electron donor with respect to tetralin as a result of the inductive effect of the methyl group. Thus, temperature effects on the activation energy in the hydrogenation of toluene may be due to a decrease in the high metal–toluene interaction energy as a result of changes in the original electronic properties of the PtPd alloy, induced by the increasing sulfur adsorption onto the metals (25) and related to the amount of sulfur in the feed.

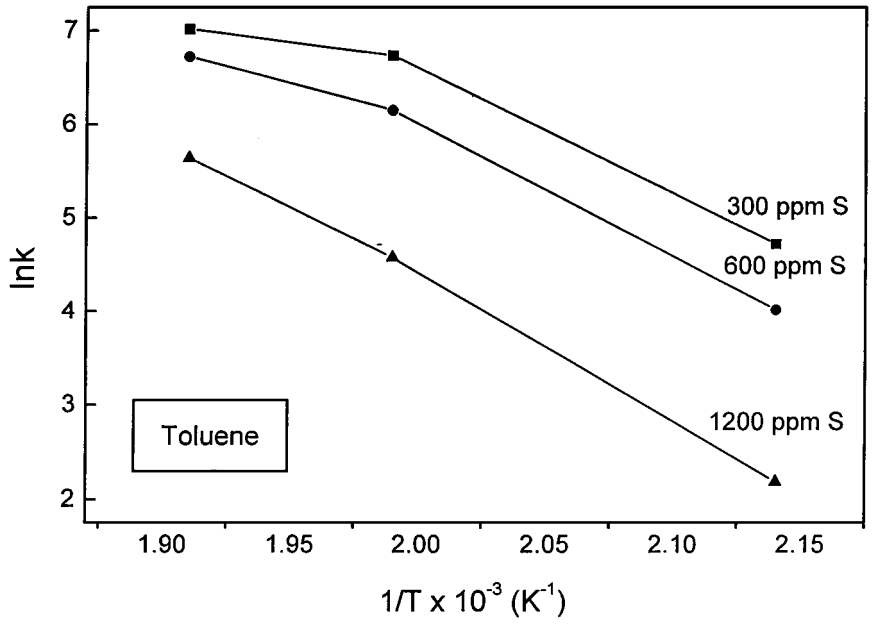

FIG. 5. Arrhenius plot for hydrogenation of toluene on PtPdx catalysts ($x = 300$–1200 ppm of S in the feed).

For toluene and tetralin hydrogenation, a convergence of activation energy and preexponetial factors were observed for the highest sulfur content (Table 5). This indicates a more homogeneous interaction of both aromatics with the metallic surface when the sulfur content in the feed is increased. Taking into account that tetralin hydrogenation is less electron-metal sensitive than its toluene counterpart, adding increasing amounts of sulfur implies that sulfur adsorption changes the electronic properties of the metal particles. The binding energies of the Pd $3d_{5/2}$ core level of PtPdx ($x = 1200$ ppm of S) catalysts support the idea that differences in activity may be mainly due to the electronic properties of the PtPd bimetallic particles.

Stringent deactivation tests were conducted on the PtPd system; the feed contained 1200 ppm of S (Fig. 7). The activity of the PtPd system was constant for 20 h of the run, indicating the high stability of the bimetallic formulation even at the high sulfur concentration used in the feed.

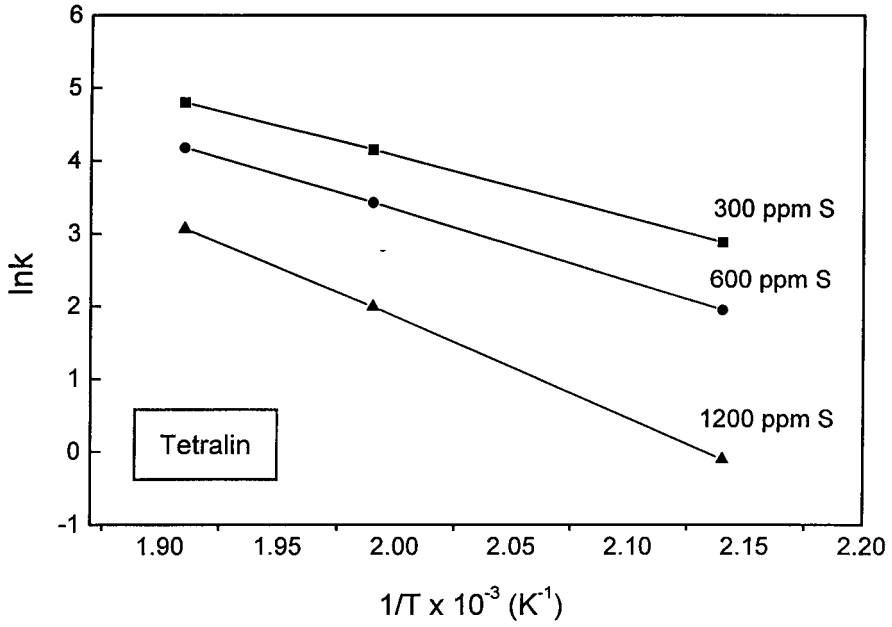

FIG. 6. Arrhenius plot for hydrogenation of tetralin on PtPdx catalysts ($x = 300$–1200 ppm of S in the feed).

TABLE 5

Arrhenius Parameters[a] for Tetralin and Toluene Hydrogenation on PtPd*x* (*x* from 300 to 1200 ppm of S in the Feed)

S (ppm)		Conversion (%)			Pseudo-rate constant (h^{-1} g_{cat}^{-1})			*T* trajectory (K)	$E_{act.}$ (kJ · mol)	ln *A*
		468 K	503 K	523 K	468 K	503 K	523 K			
300	Toluene	16.1	72.9	82.3	112.5	841	1114	468–523	*d*	*d*
	Tetralin	99.5[b] (67.3)[c]	99.7[b] (24.8)[c]	99.9[b] (7.1)[c]	18.1	63.9	121.7	468–523	70.4	21
600	Toluene	2.8	51.6	72.5	55.7	468	831	468–523	*d*	*d*
	Tetralin	99.3[b] (85.5)[c]	99.5[b] (51.0)[c]	99.7[b] (24.0)[c]	7.1	30.9	65.3	468–523	81.8	23
1200	Toluene	1.3	14.1	35.4	8.9	47.3	281	468–523	129.2	35
	Tetralin	99.1[b] (98.0)[c]	99.3[b] (85.1)[c]	99.5 (62.3)[c]	0.9	7.4	21.7	468–523	115.0	30

[a] Measured at a total pressure of 5 MPa, WHSV = 4.5 h^{-1}.
[b] Naphthalene conversion.
[c] Tetralin selectivity.
[d] Temperature-dependent activation energy, see Fig. 5.

Catalyst Structure and Activity Correlations

An analysis of the correlation between catalyst structure and activity affords several possibilities for comparing catalysts. The intrinsic activity of the hydrogenation of naphthalene and toluene in the presence of sulfur on the Pt, Pd, and PtPd/SA catalysts confirms a positive effect of Pt and Pd in the bimetallic sample, because the level of activity of this system was much higher than on either of the monometallic components. This higher intrinsic activity appears to be more closely related to the Pt–Pd interaction than to a variation in the number of metallic sites in the system. The TPR profile of the bimetallic sample, with a strong decrease in H_2 consumption associated with PdO and the appearance of a new reduction peak around 652 K, already indicates some kind of Pt–Pd interaction in the oxidic precursor.

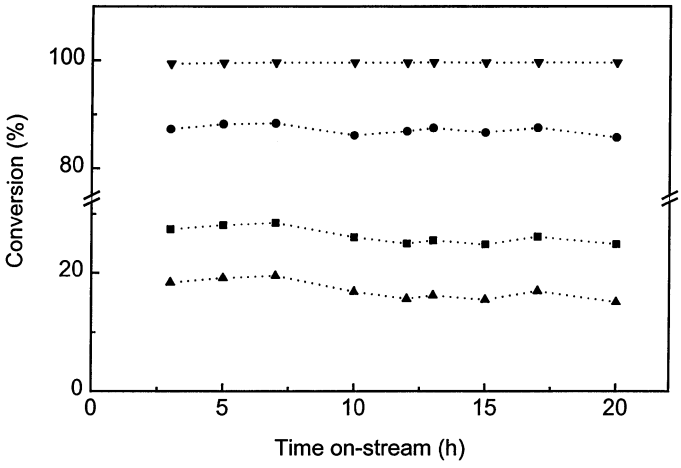

FIG. 7. Time course of total aromatics (square), DBT (circle), toluene (top triangle), and naphthalene (bottom triangle) conversions in the hydrogenation of a mixture of toluene, naphthalene, and DBT (1200 ppm of S) on a PtPd/SA catalyst. Reaction conditions: $P = 5$ MPa, $T = 523$ K, WHSV = 4.5 h^{-1}.

The infrared spectra of the reduced bimetallic sample also suggests a strong interaction of Pt and Pd. The locations of the peaks of the Pt–CO band (2103 cm^{-1}) suggest that platinum would be in an electron-deficient state in the bimetallic formulation. Since neither electronic effects associated with a strong interaction with the support nor electron transfer from the Pt to the Pd catalyst are expected, the electronic state of Pt may be related to changes in particle size (50). The strong increase in the Pt–CO absorption band, despite the lower Pt content in the PtPd catalyst, are in keeping with the above explanation. The strong Pt–Pd interaction seems to be involved in these effects since the IR spectra of CO adsorbed on Pd in the bimetallic system also show differences with respect to the monometallic Pd/SA catalyst. The shift in the linear CO band on Pd (2050 cm^{-1}) and the decrease in the linear/bridging CO ratio implies that the Pd–Pd bonds decrease in number (43) in the presence of platinum. This dilution effect of Pt on the bimetallic PtPd particles formed is also supported by the decrease in the Pd XPS signal observed in the case of the PtPd/SA catalyst. However, the stronger decrease in the surface exposure of Pd with respect to the value expected for the Pt/Pd atomic ratio introduced indicates some Pt surface segregation in the bimetallic particles, which could lead to isolated Pt clusters on the Pd surface. Surface segregation of one component (Pd) in bimetallic PtPd particles as the Pt content (Pt > 75%) increased was also found by Rades *et al.* (51).

These results clearly indicate that the catalytic behavior of PtPd/SA in the hydrogenation of aromatic compounds in the presence of sulfur is closely related to the presence of these electron-deficient Pt species (isolated Pt clusters on the Pd surface). This kind of electro-deficient metallic species is claimed by a number of researchers to be responsible for the high sulfur tolerance of supported Pt and Pd, knowing the electron acceptor character of the sulfur atom (10, 13, 52–55). The catalytic behavior of the PtPd/SA catalysts with an increase in sulfur in the feed suggests a

relationship between the electronic density of the electrodeficient Pt species and the sulfur. The electron donor character of toluene may weaken the affinity between electrondeficient Pt clusters and toluene during sulfur poisoning, leading to a decrease in the toluene-adsorption-equilibrium constant and, therefore, to a modification of the overall apparent activation energy.

In addition, the Pt agglomeration rate induced by sulfur poisoning (56), is reduced, since no differences in the XPS surface exposure of Pd, and indirectly of Pt, on the fresh samples (1200 ppm), severely poisoned by sulfur, were observed. Taking into account that the melting points of Pd and Pt sulfides are much lower than that of the metals, a sulfur-induced metallic aggregation might be expected. Consequently, the positive interaction of the bimetallic PtPd/SA catalysts may be attributed to the presence of a bimetallic interaction, which reduces the tendency of Pt to chemisorb sulfur or form bulk sulfide and its sulfur-induced metal agglomeration.

CONCLUSIONS

The hydrogenation of toluene and naphthalene in the presence of sulfur was investigated in a PtPd bimetallic catalyst under conditions which approach those used in industry, namely an overall pressure of 5.0 MPa, reaction temperature of 468 to 523 K, and a WHSV of 4.5 h^{-1}. Upon activation in hydrogen at 573 K, the bimetallic PtPd catalyst showed a higher intrinsic activity in hydrogenation in the presence of sulfur than did the monometallic Pt and Pd counterparts. When DBT (113–1200 ppm S) was introduced into the feed, the bimetallic PtPd catalyst exhibited strong resistance to poisoning by the sulfur compound. On the basis of TPR, FTIR spectra of chemisorbed CO, and XPS, it is apparent that the two metals strongly interact upon activation in hydrogen at 573 K. The exceptional performance of the PtPd catalyst with respect to its monometallic counterparts in the hydrogenation reactions is interpreted in terms of the electron-deficient platinum species (isolated Pt clusters on the Pd surface) in the resulting PtPd particles.

ACKNOWLEDGMENTS

This research was supported in part by Repsol, SA (Spain). The authors express their gratitude to Mr. J. Sánchez Caba, Repsol, SA, making it possible to publish these results. B.P. acknowledges financial support from the Consejeria de Educación y Cultura de Comunidad de Madrid (Spain).

REFERENCES

1. Absi-Halabi, M., Stanislaus, A., and Qabazard, H., *Hydrocarbon. Process.* **76**(2), 45 (1997).
2. Stanislaus, A., and Cooper, B. H., *Catal. Rev. Sci. Eng.* **36**(1), 75 (1994).
3. Cooper, B. H., and Donnis, B. B. L., *Appl. Catal. A* **137**, 203 (1996).
4. "Hart's European Fuels News," 20 February, 1998.
5. Unzelman, G. H., "AM-87-33, NPRA Annual Meeting," March 1987.
6. Yosuda, H., and Yoshimura, Y., *Catal. Lett.* **46**, 43 (1997).
7. Cooper, B. H., Stanislaus, A., and Hannerup, P. N., *Am. Chem. Soc. Div. Petrol. Chem.* **37**(1), 41 (1992). [Preprint]
8. Sogaard-Andersen, P., Cooper, B. H., and Hannerup, P. N., "AM-92-50, NPRA Annual Meeting," March 1992.
9. Barbier, J., Lamy-Pitara, E., Marecot, P., Boitiaux, J. P., Cosyns, J., and Verna, F., *Adv. Catal.* **37**, 279 (1990).
10. Gallezot, P., *in* "Catalysis by Zeolites" (B. Imelik, C. Naccache, Y. Ben Taarit, J. C. Vedrine, G. Coudurier, and H. Praliaud, Eds.), Vol. 5, p. 227. Elsevier Science, Amsterdam, 1980.
11. Yasuda, H., Sato, T., and Yoshimura, Y., *Am. Chem. Soc. Div. Petrol. Chem.* **42**(3), 580 (1997). [Preprint]
12. Tri, T. M., Massardier, J., Gallezot, P., and Imelik, B., *in* "Metal-support and Metal Additives Effects in Catalysis" (B. Imelik, C. Naccache, G. Coudurier, H. Praliaud, M. Meriaudeau, P. Gallezot, G. A. Martin, and J. C. Vedrine, Eds.), Vol. 11, p. 141. Elsevier, Amsterdam, 1982.
13. Sachtler, W. M. H., and Stakheev, A. Yu., *Catal. Today* **12**, 283 (1992); Homeyer, S. T., and Sachtler, W. M. H., *Stud. Surf. Sci. Catal.* **49**, 975 (1989).
14. Hoyos, L. J., Primet, M., and Praliaud, H., *J. Chem. Soc. Faraday Trans.* **88**(1), 113 (1992).
15. Lin, S. D., and Vannice, M. A., *J. Catal.* **143**, 563 (1993).
16. Rahaman, M. V., and Vannice, M. A., *J. Catal.* **127**, 251, 267 (1991).
17. Figueras, F., Gomez, R., and Primet, M., *Adv. Chem. Ser.* **121**, 480 (1973).
18. Phuong, T. T., Massardier, J., and Gallezot, P., *J. Catal.* **102**, 456 (1986).
19. Szymanski, R., Charcosset, H., Gallezot, P., Massardier, J., and Tournayan, L., *J. Catal.* **97**, 366 (1986).
20. Poondi, D., and Vannice, M. A., *J. Catal.* **161**, 742 (1996).
21. Chou, P., and Vannice, M. A., *J. Catal.* **107**, 140 (1987).
22. Koussathana, M., Vamvouka, D., Economou, H., and Verykios, X., *Appl. Catal.* **77**, 283 (1991); Koussathana, M., Vamvouka, D., Tsapatsis, M., and Verykios, X., *Appl. Catal.* **80**, 99 (1992).
23. Lin, D., and Song, C., *Catal. Today* **31**, 93 (1996).
24. Chiou, J. F., Huang, Y. L., Lin, T. B., and Chang, J. R., *Ind. Eng. Chem. Res.* **34**, 4277 (1995).
25. Guenin, M., Breysse, M., Frety, R., Tifouti, K., Marecot, P., and Barbier, J., *J. Catal.* **105**, 144 (1987).
26. Kovach, S. M., and Wilson, G. D., U.S. patent 3 943 053 (1974), to Ashland Oil, Inc.
27. Kukes, S. G., Clark, F. T., Hopkins, P. D., and Green, L. M., U.S. patent 5 151 172 (1991), to Amoco Corp.
28. Minderhoud, J. K., and Lucien, J. P., European Patent 303 332 (1988), to Shell IRM.
29. Winquist, B. H. C., Milam, S. N., Murray, B. D., and Ryan, R. C., European patent 92-201799 (1992), to Shell IRM.
30. Sinfelt, J. H., *J. Catal.* **29**, 308 (1973).
31. Jenck, J., and Germain, J. E., *J. Catal.* **65**, 141 (1980).
32. Cosyns, J., Franck, J. P., and Gil, J. M., *C.R. Acad. Sci.*, Paris **287**C, 85 (1978).
33. Gates, B. C., Katzer, J. R., and Schuit, G. C. A., "Chemistry of Catalytic Processes," p. 39. McGraw Hill, New York, 1979.
34. Lietz, G., Lieske, H., Spindler, H., Hanke, W., and Wolter, J., *J. Catal.* **81**, 17 (1983).
35. Kokayeff, P., "Catalyst Hydroprocessing of Petroleum Distillates," p. 315. Dekker, New York, 1994.
36. Huang, T. C., and Kung, B. C., *Ind. Eng. Chem. Res.* **34**, 1140 (1995).
37. Chen, G., Chou, W.-T., and Yeh, C.-T., *Appl. Catal.* **8**, 389 (1983).
38. Noronha, F. B., Schmal, M., Primet, M., and Fréty, R., *Appl. Catal.* **78**, 125 (1991).
39. Soma-Noto, Y., and Sachtler, W. M. H., *J. Catal.* **32**, 315 (1974).
40. Apesteguia, C. R., Brema, C. E., Garetto, T. F., Borgna, A., and Parera, J. M., *J. Catal.* **89**, 52 (1984).
41. Otten, M. M., Clayton, M. J., and Lamb, H. H., *J. Catal.* **149**, 211 (1994).
42. Gelin, P., Siedle, A. R., and Yates, J. T., *J. Phys. Chem.* **88**, 2978 (1984).

43. Eishens, R. P., and Pliskin, W. A., *Adv. Catal.* **10**, 2 (1958).
44. Otto, K., Haack, L. P., and de Vries, J. E., *Appl. Catal. B* **1**, 1 (1992).
45. Vedrine, J. C., Dufaux, M., Naccache, C., and Imelik, B., *J. Chem. Soc. Faraday Trans. I* **74**, 440 (1978).
46. Rahman, M. V., and Vannice, M. A., *J. Catal.* **127**, 267 (1991).
47. Moreau, C., and Geneste, P., *in* "Theoretical Aspects of Heterogeneous Catalysis" (J. B. Moffat, Ed.), p. 256. Van Nostrand Reinhold, New York, 1990.
48. Singhal, G. H., Espino, R. L., Sobel, J. E., and Huff, G. A., *J. Catal.* **67**, 457 (1981).
49. Van Santen, R. A., and Niemantsverdriet, J. W., *in* "Chemical Kinetics and Catalysis." Plenum, New York, 1995.
50. Miller, J. T., and Koningsberger, D. C., *J. Catal.* **162**, 209 (1996).
51. Rades, T., Pak, C., Polisset-Thfoim, M., Ryoo, R., and Fraissard, J., *Catal. Lett.* **29**, 91 (1991).
52. Dalla Betta, R. A., and Boudart, M., *in* "Proceedings, 5th International Congress on Catalysis, Palm Beach, 1972" (J. W. Hightower, Ed.), Vol. 2, p. 1329. North Holland, Amsterdam, 1973)
53. Gallezot, P., *Catal. Rev. Sci. Eng.* **20**, 121 (1979).
54. Lin, T.-B., Jan, C.-A., and Chang, J.-R., *Ind. Eng. Chem. Res.* **34**, 4284 (1995).
55. Lee, J. K., and Rhee, H. K., *J. Catal.* **177**, 208 (1998).
56. Vaarkamp, M., Miller, J. T., Modica, F. S., Lane, G. S., and Koningsberger, D. C., *J. Catal.* **138**, 675 (1992).